J Mater Sci: Mater Electron (2017) 28:16426–16432
DOI 10.1007/s10854-017-7553-7

Effect of donor and acceptor co-doping in $(Na_{0.52}\ K_{0.48})\ (Nb_{0.95}\ Sb_{0.05})O_3$ lead-free piezoceramic

Bhupender Rawal[1] · N. N. Wathore[1] · B. Praveenkumar[1] · H. S. Panda[2]

Received: 16 May 2017 / Accepted: 17 July 2017 / Published online: 25 July 2017

Abstract The study highlights the effect of donor (Sr^{2+}) and acceptor (Zr^{4+}) co-doping on phase formation, microstructure, density, ferroelectric, dielectric, piezoelectric, fatigue and aging properties of $(Na_{0.52}\ K_{0.48})(Nb_{0.95}\ Sb_{0.05})O_3$, abbreviated as NKNS, lead free piezoelectric ceramics. The composition (1–x)(NKNS)—x$SrZrO_3$ (where x = 0.0, 0.02, 0.04, 0.06 and 0.08) were synthesized by mixed oxide route. The doping drastically affected the phase formation and the microstructure. The poling studies suggested that the material requires higher poling temperature (120 °C) for optimum properties. At the small concentration of $SrZrO_3$, the dominant effect of acceptor doping induced '*hybrid*' piezoelectric behavior which improved fatigue, ageing and piezoelectric properties. The mechanical quality factor (Q_m) more than doubled (96) and piezoelectric charge co-efficient peaked to 157×10^{-12} C/N for 2% $SrZrO_3$. The study of Raman spectra ascertained that the doping influenced the nature of B–O bonding. The electrical fatigue behavior in conjunction with ferroelectric studies confirmed that due to complex doping different mechanisms work to stabilize the polarization state which influenced the ageing and fatigue behavior.

✉ Bhupender Rawal
bsrawal@arde.drdo.in

[1] Armament Research and Development Establishment, Pune 411021, India

[2] Defence Institute of Advanced Technology, Pune 411025, India

1 Introduction

Piezoelectric lead zirconate titanate (PZT) ceramics are widely used in many applications like sensors, transducer and actuators because of high piezoelectric and dielectric properties [1]. However, the use of lead based ceramics has caused serious environmental problem. The toxicity of lead containing piezoceramics is a serious issue. Hence, there was a great need to replace PZT with lead free piezoelectric material having good piezoelectric and dielectric properties [2, 3]. Along with it, good resistance to ageing and electrical fatigue is also desired for electronics application [1].

Alkaline niobate based materials are one of the promising candidate, among the lead free materials, to replace lead based piezoelectric materials. But still the piezoelectric properties of NKN materials are inferior to the PZT. The piezoelectric properties of $(k_{0.5}\ Na_{0.5})(Nb_{(1-y)}Sb_y)O_3$ was studied by Gong et al. [4], which confirmed good piezoelectric properties with a d_{33} of 134×10^{-12} C/N. However, the properties can be modulated, as required, for different application by incorporating "hard" or "soft" dopant in the perovskite NKNS materials. The addition of acceptor "hard" dopant, like Zr^{4+} [5] replacing Nb^{5+} or Sb^{5+} in NKN perovskite structure, creates oxygen vacancies which enhances coercive field (E_C) and electromechanical quality factor (Q_m) due to the formation of defect dipoles between the acceptor ions and charge compensating oxygen vacancies [6–9]. On the other hand, donor "soft" dopant, like Sr^{2+} [10] replacing K^+ or Na^+, inhibits oxygen vacancies formation which decreases E_C and Q_m and enhances piezoelectric properties [7, 11]. As compared to PZT, co-doping of acceptor and donor has not been studied so elaborately in NKN based system [12, 13]. The ageing and fatigue behavior plays a pivotal role in fabrication of sensor

devices as these may alter the properties and functionality significantly.

Therefore, in our study, there is a co-doping of Sr at A-site and Zr at B-site in NKNS, which acts as a soft and hard dopant, respectively, and efforts have been made to unravel the effects of such co-doping on the properties of NKNS through ferroelectric, microstructural and phase formation studies. Due emphasize has been given on fatigue and ageing characteristics of co-doped samples. We have endeavored to explain how it influences the poling behavior, ferroelectric, piezoelectric, electrical fatigue, ageing properties etc. and the mechanisms involved.

2 Experimental

Lead free $(1-x)$ $(Na_{0.52}\ K_{0.48})$ $(Nb_{0.95}\ Sb_{0.05})O_3$—x $SrZrO_3$ ceramics, x = 0.00–0.08, were produced by conventional solid state reaction method. The $(Na_{0.52}\ K_{0.48})$ $(Nb_{0.95}\ Sb_{0.05})O_3$ was prepared from powders of Potassium carbonate (K_2CO_3), Sodium carbonate (Na_2CO_3), Antimony pentoxide (Sb_2O_5) and Niobium pentoxide (Nb_2O_5), (Sigma-Aldrich, purity ≥ 99.8%), which were mixed in planetary ball mill with zirconia grinding media for 24 h. Subsequently, the powder was calcined at 800 °C for 5 h. Similarly, $SrZrO_3$ (abbreviated as SZ) was prepared separately from Strontium carbonate ($SrCO_3$) (Sigma-Aldrich, purity ≥ 99.8%) and Zirconium oxide (ZrO_2) (IRE, purity 99.5%) by calcining at 1070 °C for 3.5 h. Then the NKNS and SZ powders were mixed and milled for 24 h in stoichiometric ratio and calcined at 800 °C for 3 h to form $(Na_{0.52}\ K_{0.48})$ $(Nb_{0.95}\ Sb_{0.05})O_3$, $0.98(Na_{0.52}\ K_{0.48})$ $(Nb_{0.95}\ Sb_{0.05})O_3$—$0.02SrZrO_3$, $0.96(Na_{0.52}\ K_{0.48})$ $(Nb_{0.95}\ Sb_{0.05})O_3$—$0.04SrZrO_3$, $0.94(Na_{0.52}\ K_{0.48})$ $(Nb_{0.95}\ Sb_{0.05})O_3$—$0.06SrZrO_3$ and $0.92(Na_{0.52}\ K_{0.48})$ $(Nb_{0.95}\ Sb_{0.05})O_3$—$0.08SrZrO_3$ ceramics, henceforth referred to as NKNS, 2SZ, 4SZ, 6S and 8SZ, respectively. Samples in the form of disc of diameter 10 mm were pressed by double acting hydraulic press (Make GMT) at 110 MPa. Then disc were sintered at 1140 °C for 3 h in closed alumina crucible. The sintered samples were lapped to the thickness of 1.2 mm and the densities were determined by Archimedes method. The crystalline phase formation was analyzed using X-ray diffractometer, D8 Advance (Make Bruker AXS GmbH). The microstructure of the fractured surface of the sintered samples was explored using FESEM, Merlin (Make Carl Zeiss) and the Quantimet software was employed to carry out the grain size measurements. For the electrical measurements, silver electrodes were applied on both the surfaces of the sintered samples. The ferroelectric and fatigue behavior were determined at room temperature using aix ACCT TF 2000 analyzer. Dielectric constant and loss tangent (tan δ) was measured using LCR HiTESTER (HIOKI 3532, Japan). Samples were poled at different poling temperatures using high DC power supply (Glassman). The piezo d_{33} meter (Piezotest PM300) was engaged to measure piezoelectric charge coefficient (d_{33}) and the same instrument was used for carrying out the aging study by measuring the d_{33} at different time intervals after poling. The Raman spectroscopy was conducted using the 514 nm line of an Ar—laser (300 mW) (inVia Reflex, Renishaw UK) at the room temperature.

3 Results and discussion

The X-ray diffraction profiles of $SrZrO_3$ and NKNS-SZ compositions are shown in Fig. 1. $SrZrO_3$ belongs to the perovskite family. It has an orthorhombic structure with space group *Pbnm* and xrd pattern was matching JCPDS card No. 70-0283, thus, indexed accordingly [14, 15]. XRD profile shows pure perovskite phase formation without any presence of secondary phases, implying that the Sr and Zr are fully soluble in the NKNS lattice in the range studied. The substitution of Zr^{4+} ($R_{Zr}^{4+} = 72$ pm) having larger ionic diameter than the cations Nb^{5+} ($R_{Nb}^{5+} = 64$ pm) and Sb^{5+} ($R_{Sb}^{5+} = 60$ pm) [16], is expected to shift the peaks at lower 2θ value due to increase of the lattice volume. Whereas, Sr^{2+} ($R_{Sr}^{2+} = 144$ pm) substitution at A-site should yield opposite trend as interplanar spacing (*d*) will get shortened. It is observed that the peaks shift to higher 2θ values as SZ content increase and then starts decreasing beyond 4SZ, which suggests that effect of Sr^{2+} substitution at A-site for Na^+/K^+ yields more influence at lower doping percentage.

Figure 2a–e shows scanning electron microscopy (SEM) of the fractured surface of the samples sintered at

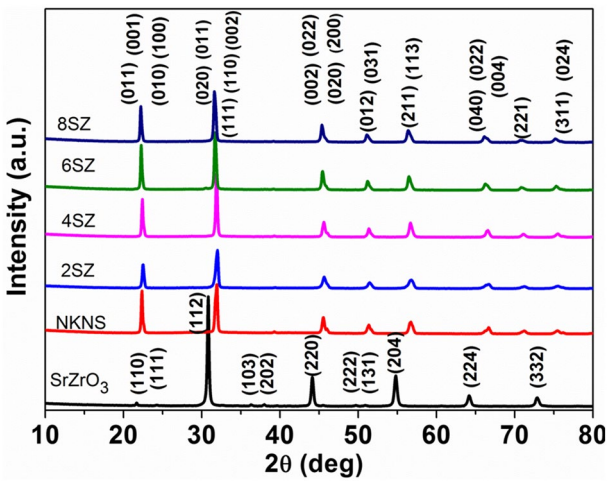

Fig. 1 X-ray diffraction profile of $SrZrO_3$ (calcined) and $(1-x)$ NKNS-xSZ ceramics sintered at 1140 °C

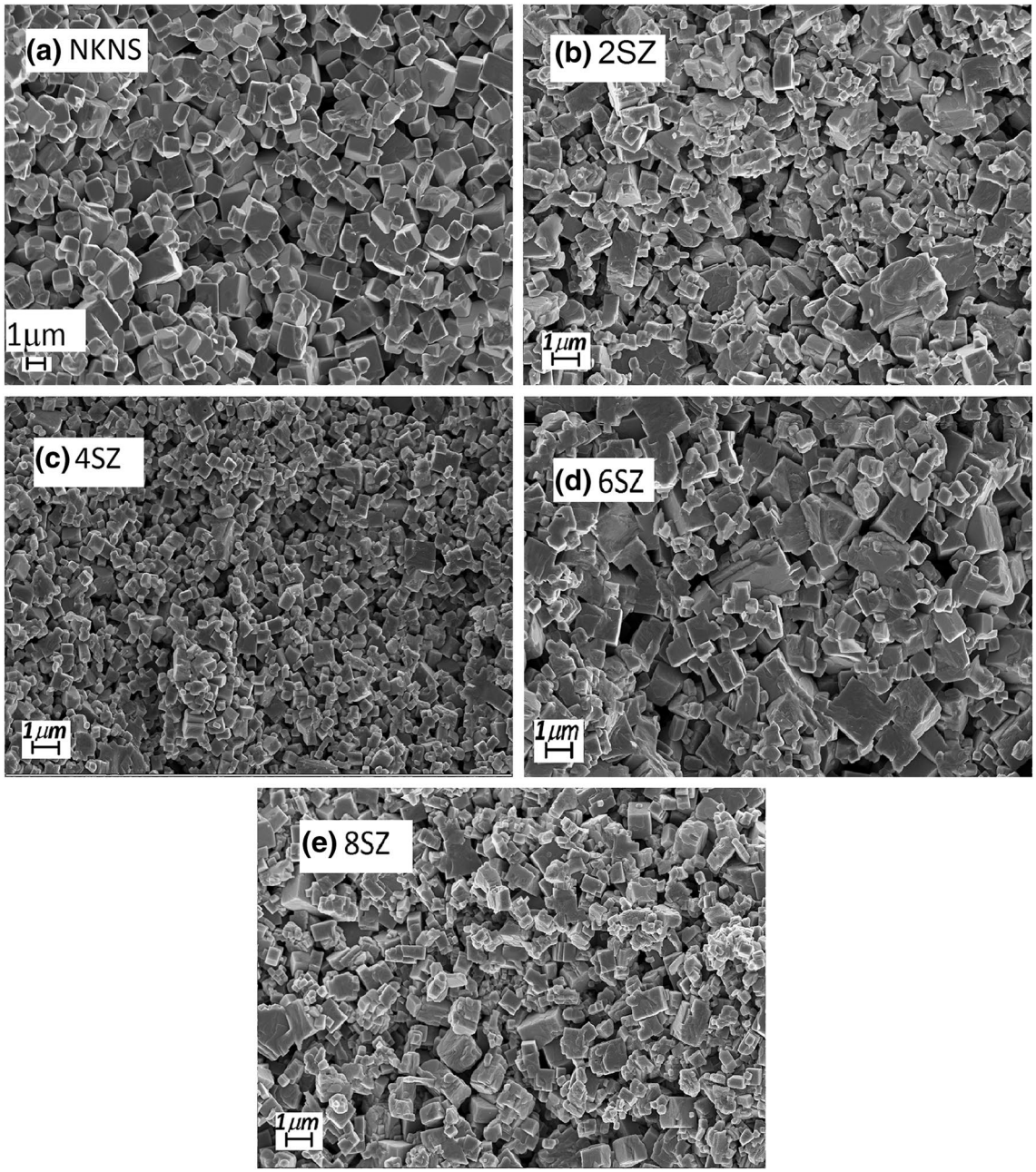

Fig. 2 **a–e** Scanning electron micrograph of fractured surface of (1 – x)NKNS-xSZ ceramics sintered at 1140 °C

1140 °C/3 h. The SEM of NKNS shows typical morphology having bimodal grain size distribution with cubical grains. Coarse grains with average size of 1.678 μm are found interspersed between fine grains having an average size of 0.788 μm. As can be seen, as the concentration of SZ increases, the grain size as well as the number of coarse grains starts decreasing. The grain boundaries are not sharp and average size of grains is about 1.3127 μm for 2SZ sample. In 4SZ sample, grain size further reduces to 0.4768 μm. Reducing grain size with increasing SZ content implies that donor effect are more prominent here [11, 12]. With the further increase of the SZ content, microstructure hints of particle amalgamating together to form bigger particles of average size 1.417 μm which points toward increased acceptor dopant .i.e. Zr^{4+} influence. The morphology of grains, however, remains cubical only. This shows that the grains are heterogeneously distributed in the matrix. The uneven grain growth may also be due to contest between liquid phase sintering, encouraging densification and A-site cation vacancies

which promotes fine grains' growth and inhibits densification [17].

Figure 3 shows the piezoelectric charge coefficient (d_{33}) for different compositions, poled at various temperature ranging from room temperature (RT) to 140 °C. The poling field applied was 3 kV/mm for 1 h. The d_{33} increased for all the samples with increase in poling temperature. After reaching maxima at 120 °C it saturates and does not show any significant increase at higher temperature. The highest d_{33} of 157×10^{-12} C/N was observed for the 2SZ sample. It is clearly observed from the studies that the material requires higher poling temperature. The NKNS-SZ ceramics gives optimal properties at higher poling temperature due to favorable lattice distortion and ease of reorientation of domains which maximizes the number of dipoles aligned in the poling direction [18, 19]. However, there is no significant change in property beyond 4SZ.

The ferroelectric behavior of the ceramics samples at room temperature along with the switching current pattern of the respective loop is shown in Fig. 4 and its inset. All the samples exhibited unsaturated ferroelectric loop and slight lossy capacitor behavior. The NKNS displayed coercive field of (E_c) of 0.87 kV/mm and remnant polarization (P_r) of 31 μC/cm^2, respectively. By increasing the concentration of SZ mol% from 2 to 4, E_C increases to 1.46 kV/mm with a decrease in P_r value to 20 μC/cm^2. The reason for this is probably that, at lower concentration of SZ, Sr^{2+} is utilized in filling up the vacancies created due to volatilization of A-site cations, having low atomic mass, during sintering. While, Zr^{4+} replaced Nb^{5+}/Sb^{5+} and generated negatively charged centers ($Zr'_{Sb/Nb^{5+}}$), and to counter-balance it the positively charged oxygen vacancies ($V_O^{\cdot\cdot}$) are formed as follows:

$$O_0 = \frac{1}{2}O_2\,(g) + V_O^{\cdot\cdot} + 2e' \quad (1)$$

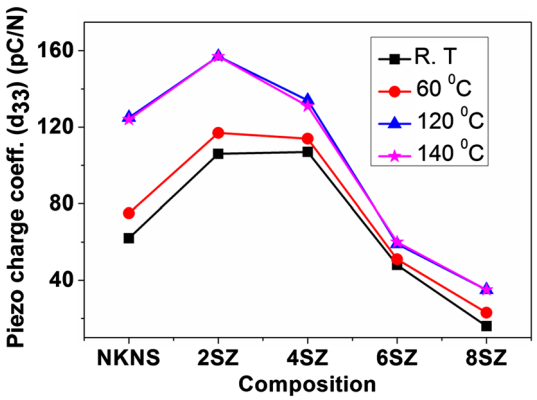

Fig. 3 Piezoelectric charge co-efficient (d_{33}) of (1 − x)NKNS-xSZ ceramics after poling at different temperatures. (Color figure online)

where e' represents an electron and $V_O^{\cdot\cdot}$ is oxygen vacancy with two effective positive charges. Therefore, the defect dipoles were formed with the charge compensating oxygen vacancies which acts as pinning centers, thereby restricting the domain motion leading to the hard ferroelectric effect [20, 21]. An inner bias field is also formed which tends to reverse the switching polarization leading to a decreased value of P_r [22]. The fact that the 2SZ sample has highest mechanical quality factor (Qm) value, as can be seen in Table 1, lends more credibility to above proposition. This implies that the domain wall pinning is strongest in it and reduces as SZ content increases. On comparing the piezoelectric and ferroelectric properties it can be concluded that complex doping of acceptor and donor has bestowed "*hybrid*" properties to 2SZ samples [12]. At still higher doping of SZ, E_c and Pr decreased to 0.7 kV/mm and 2 μC/cm^2, respectively, which are less than the undoped samples. The decrease in E_C values can be attributed to the decrease of oxygen vacancies due to the reduction in oxygen vacancies by the donor effect because as the concentration of SZ increases more and more $Sr^{\cdot}_{Na/K^{+1}}$sites are created due to substitution of Sr^{2+} at Na^{1+}/K^{1+} site. The decrease in P_r, however, can be attributed to the fact that the overall effect of SZ doping leads to decrease in spontaneous

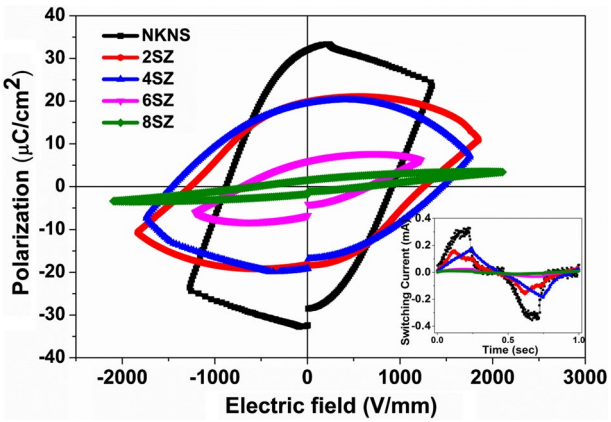

Fig. 4 Ferroelectric loop (Polarization vs. Electric field) of sintered (1 − x)NKNS-xSZ samples. (*Inset* shows the switching current behavior for same ceramic samples). (Color figure online)

Table 1 Dielectric constant (K^T_3), Tan δ, Q_m and electromechanical coupling coeff. (k_p) for (1 − x)NKNS-xSZ samples

Composition	K^T_3	Tan δ	Q_m	k_p (%)
NKNS	927	0.125	44	41
2SZ	760	0.71	96	35
4SZ	642	0.82	86	33
6SZ	536	0.59	51	30
8SZ	488	0.19	32	29

polarization (P_S) of the samples, probably because more and more distortion is created in the lattice structure as Sr^{2+} ($R_{Sr}^{2+}=144$ pm) and Zr^{4+} ($R_{Zr}^{4+}=72$ pm) gets substituted in place of Na^+/K^+ ($R_{Na}^{+}=139$ pm, $R_K^{+}=164$ pm) and Nb^{5+}/Sb^{5+} ($R_{Nb}^{5+}=64$ pm ,$R_{Sb}^{5+}=60$ pm), respectively [16]. The *tolerance factor* values can shed some light on this aspect which was given by Goldschmidt in 1926 [23] as:

$$t = (R_O + R_A)/\sqrt{2}(R_O + R_B) \quad (2)$$

where R_o, R_A and R_B are the ionic radii of A, B and O atom in ABO_3 perovskite formula. For $(1-x)((Na_{0.52}K_{0.48})Nb_{0.95}Sb_{0.05})O_3$—$xSrZrO_3$ ceramic, tolerance factor equation takes the following form:-

$$t = \frac{\left[R_{O^{2-}} + \left\{\left(0.52 - \frac{x}{2}\right)R_{Na^+} + \left(0.48 - \frac{x}{2}\right)R_{K^+} + xR_{Sr^{2+}}\right\}\right]}{\left[\sqrt{2}\left(R_{O^{2-}} + \left\{\left(0.95 - \frac{x}{2}\right)R_{Nb^{5+}} + \left(0.05 - \frac{x}{2}\right)R_{Sb^{5+}} + xR_{Zr^{4+}}\right\}\right)\right]} \quad (3)$$

where $R_O^{2-}=140$ pm, $R_{Na}^{+}=139$ pm, $R_K^{+}=164$ pm, $R_{Nb}^{5+}=64$ pm, $R_{Sb}^{5+}=60$ pm, $R_{Sr}^{2+}=144$ pm and $R_{Zr}^{4+}=72$ pm [16]. The tolerance factor for pure NKNS is 1.009809 which decreases continuously and reaches the value of 1.004632 for 8SZ. It implies that, theoretically, the lattice is progressing towards centrosymmetric cubic structure. This can be corroborated from the switching current behavior also which displays decreased switching current value, indicating that the number of switchable domains is reduced.

The Raman spectrum of different compositions is shown in Fig. 5 where $\upsilon 1(1A_{1g})+\upsilon 2(1E_g)+\upsilon 3\ (F_{1u})$ are stretching and $\upsilon 5\ (F_{2g})$ is bending modes of BO_6 octahedra. The peaks below wavenumber 200 cm^{-1} are due to rotation of BO_6 octahedra and translation modes of ionic A-site cations [24]. It can be seen that as SZ content increases the broadness of the bands increases from NKNS to 8SZ which can be assigned to the random orientation of grains, disorder at A-site and overlapping of the Raman bands. At higher SZ concentration there is a decrease of intensity of the bands above 200 cm^{-1} which indicates that the B–O bond is becoming less polarizable. This is primarily because as Zr^{4+}, which is more electropositive than Nb^{5+}/Sb^{5+}, is getting substituted in the lattice, the covalent nature of B–O bond reduces making it less polarizable, which consequently diminish the ferroelectric characteristics and dips the scattering intensity [25]. However, the decrease in intensity of the bands below 200 cm^{-1} is due to the heavier mass of Sr^{2+} ion as compared to Na^+/K^+ which makes the translational movement difficult. The decrease in scattering intensity also points to the fact that the strength of *p–d* hybridization is reduced. Perhaps, the electrons generated on acceptor doping are occupying the *d*-orbital of B-cation, thereby, reducing the bonding between *4d* orbital of B-site cation and *2p* orbital of O anion which is highly essential for ferroelectricity [26]. The absence of *p–d* interaction favors the cubic structure [26], as was observed through tolerance factor values too, which encourages non-ferroelectric characteristics.

Figure 6 shows the aging of the d_{33} for all SZ doped NKNS material poled at 120 °C. The degradation of the piezoelectric properties with time, in the absence of any mechanical or electrical load [27], is called as ageing. All

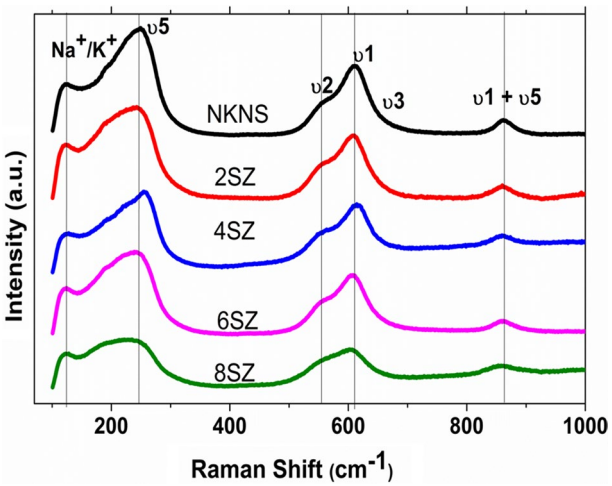

Fig. 5 Raman spectrum of (1 – x)NKNS- xSZ ceramics

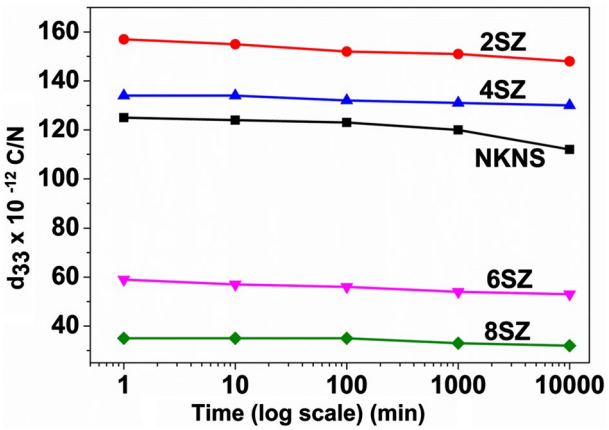

Fig. 6 Ageing behavior of (1 – x)NKNS-xSZ ceramics

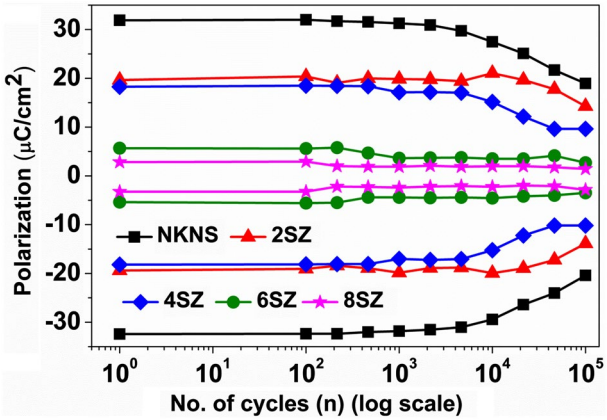

Fig. 7 Electrical fatigue behavior of (1 − x)NKNS-xSZ ceramics. (Color figure online)

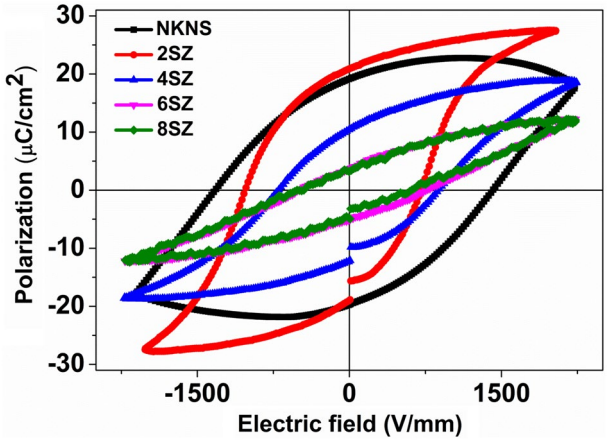

Fig. 8 P–E loop of (1 − x)NKNS-xSZ ceramics after electrical fatigue. (Color figure online)

the samples exhibited stable piezoelectric properties for the studied time, which is quite promising for device application. As compared to NKNS, SZ doped samples are more stable because of generated defect dipoles which stabilize the polarization state of domains by clamping them [28]. These defect dipoles resist the crystal spontaneous polarization from switching back to original state when the electric field is removed.

Figure 7 exhibits the electrical fatigue behavior for NKNS-SZ ceramics. Similar to ageing, the fatigue behavior also improved for higher SZ content. To understand the results better, polarization studies were carried out on fatigued samples. Figure 8 exhibits the polarization loops of fatigued samples. Prima facie, it can be seen that electrical fatigue has influenced the ferroelectric loop drastically, especially for NKNS. The lossy capacitor behavior has vanished after exposing the samples to cyclic electrical loading because during electrical fatigue cycle there is generation as well as redistribution of oxygen vacancies which has clamped the charge carriers. Slight loop relaxation behavior was seen in 6SZ and 8SZ samples [29], probably due to unpinning and redistribution of vacancies and charge carriers during cyclic loading. As was expected, the 2SZ exhibited least deterioration in properties because of its *hybrid* behavior with maximum Q_m due to clamping of domain walls, which resisted the drop in P_r. Despite having softness with low Q_m value (32) the 8SZ sample displayed superior fatigue resistance which suggest that rather than domain pinning mechanism it is the reduced number of ferroelectric domains which led to fatigue-free behavior in 8SZ sample [30].

4 Conclusion

The SZ doping in lead free NKNS based piezoelectric material has substantial effects on phase formation, microstructure, piezoelectric and dielectric properties. The material required higher poling temperature to achieve maximum piezoelectric properties. The lower SZ doping increases piezoelectric properties, coercive field and mechanical quality factor. The ageing and bipolar fatigue resistance improved tremendously by SZ doping. Two different mechanisms were identified behind this improved resistance: first, effect of Zr^{4+} as acceptor at low dopant concentration, and second, the reduced number of ferroelectric domains at higher level. The properties are influenced by the number of space charge or vacancies generated at different concentration. It was concluded that a small concentration of SZ produces "*hybrid*" effect while higher concentration endows "soft" properties to ceramics. The doping elements alter the nature of B–O bonding which influences the overall properties.

Acknowledgements The authors express their sincere gratitude to Director, Armament Research and Development Establishment for extending his support for this work.

References

1. G.H. Heartling, J. Am. Ceram. Soc. **82**(4), 797 (1999). doi:10.1111/j.1151-2916.1999.tb01840.x
2. S.T. Lau, C.H. Cheng, S.H. Choy, D.M. Lin, K.W. Kwok, H.L.W. Chan, J. Appl. Phys. **103**, 104105 (2008). doi:10.1063/1.2927252
3. P. Kumari, R. Rai, S. Sharma, M. Shandilya, A. Tiwari, Adv. Mater. Lett. **6**, 453 (2015). doi:10.5185/amlett.2015.4086
4. Y. Gong, G. Yang, X. Li, L. Gong, L. Li, J. Peng, X. Zheng, J. Mater. Sci. **23**, 1910 (2012). doi:10.1007/s10854-012-0879-2
5. X. Vendrell, J.E. Gorcia, X. Brill, D.A. Ochoa, L. Mestres, G. Dezanneau, J. Eur. Ceram. Soc. **35**, 125 (2015). doi:10.1016/j.jeurceramsoc.2014.08.033

6. J.B. Lim, S. Zhang, J.-H. Jeon, T.R. Shrout, J. Am. Ceram. Soc. (2010). doi:10.1111/j.1551-2916.2009.03528.x
7. B. Jaffe, W.R. Cook Jr., H. Jaffe, *Piezoelectric Ceramics* (Academic Press, London and New York, 1971), pp. 150–250
8. R.A. Eichel, H. Kungl, M.J. Hoffmann, J. Appl. Phys. **95**, 8092 (2004). doi:10.1063/1.1728310
9. R.A. Eichel, P. Erhart, P. Traskelin, K. Albe, H. Kungl, M.J. Hoffmann, Phys. Rev. Lett. **100**, 095504 (2008). doi:10.1103/PhysRevLett.100.095504
10. B. Malic, J. Bernard, J. Holc, D. Jenko, M. Kosec, J. Eur. Ceram. Soc. **25**, 2707 (2005). DOI:10.1016/j.jeurceramsoc.2005.03.127
11. N.M. Hagh, B. Jadidian, E. Ashbahian, A. Safari, IEEE Trans. Ultrason. Ferroelectr. FrEq. Control **55**(1), 212 (2008). doi:10.1109/TUFFC.2008.630
12. B.W. Lee, E.J. Lee, J. Electroceram. **17**, 597 (2006). doi:10.1007/s10832-006-8568-2
13. E. Erdem, R.A. Eichel, H. Kungl, M.J. Hoffmann, A. Ozarowski, J. V. Tol, L.C. Brunel, IEEE Trans. Ultrason. Ferroelectr. FrEq. Control **55**(5), 1061 (2008). doi:10.1109/TUFFC.2008.757
14. B.J. Kennedy, C.J. Howard, B.C. Chakoumakos, Phys. Rev. B **59**(6), 4023 (1999). doi:10.1103/PhysRevB.59.4023
15. A. Ahtee, M. Ahtee, A.M. Glazer, A.W. Hewat, J. Acta Crystallogr. **B32**, 3243 (1976). doi:10.1107/S0567740876010029
16. R.D. Shannon, Acta Cryst. A **32**, 751 (1976). doi:10.1107/S0567739476001551.
17. R. Zuo, M. Wang, B. Ma, J. Fu, T. Li, J. Phys. Chem. Solids **70**, 750 (2009). doi:10.1016/j.jpcs.2009.03.003
18. Q. Li, M.H. Zhang, Z.X. Zhu, K. Wang, J.S. Zhou, F.Z. Yao, J.F. Li, J. Mater. Chem. C **5**, 549 (2017). doi:10.1039/C6TC04723H
19. J.L. Jones, B.J. Iverson, K.J. Bowman, J. Am. Ceram. Soc. **90**(8), 2297 (2007). doi:10.1111/j.1551-2916.2007.01820.x
20. Y. Li, J. Yuan, D. Wang, D. Zhang, H. Jin, M. Cao, J. Am. Ceram. Soc. **96**(11), 3440 (2013). doi:10.1111/jace.12479
21. S. Zhang, J.B. Lim, H.J. Lee, T.R. Shrout, IEEE trans. Ultrason. Ferroelectr. FrEq. Control **56**(8), 1523 (2009). doi:10.1109/TUFFC.2009.1215
22. H.E. Mgbemere, R.P. Herber, G.A. Schneider, J. Eur. Ceram. Soc. **29**(9), 1729 (2009). doi:10.1016/j.jeurceramsoc.2008.10.012
23. V.M. Goldschmidt, Naturwissenschaften **21**, 477 (1926). DOI:10.1007/BF01507527
24. Y. Na, J. Abolfazl, Z. Lanling, G. Zhigang, C. Zhenxiang, W. Xiaolin, J. Alloys Compd. **652**, 341 (2015). doi:10.1016/j.jallcom.2015.08.222
25. R.C. Cohen, Nature **358**, 136 (1992). doi:10.1038/358136a0
26. M.M. Shamim, T. Ishidate, K. Ohi, J. Phys. Soc. Jpn. **72**(3), 551 (2003). doi:10.1143/JPSJ.72.551
27. H. Birol, D. Damjanovic, N. Setter, J. Eur. Ceram. Soc. **26**, 861 (2006). doi:10.1016/j.jeurceramsoc.2004.11.022
28. U. Robels, G. Arlt, J. Appl. Phys. **73**, 3454 (1993). doi:10.1063/1.352948
29. K. Carl, K.H. Hardtl, Ferroelectrics **17**, 473 (1977). doi:10.1080/00150197808236770
30. Z. Luo, T. Granzow, J. Glaum, W. Jo, J. Rödel, M. Hoffman, J. Am. Ceram. Soc. **94**(11) 3927 (2011). doi:10.1111/j.1551-2916.2011.04605.x